Energy Conversion and Management 86 (2014) 992–1000

Contents lists available at ScienceDirect

Energy Conversion and Management

journal homepage: www.elsevier.com/locate/enconman

Simulation and evaluation of a CCHP system with exhaust gas deep-recovery and thermoelectric generator

J.L. Wang, J.Y. Wu *, C.Y. Zheng

Institute of Refrigeration and Cryogenics, Shanghai Jiao Tong University, Dongchuan Road 800, Shanghai 200240, China

ARTICLE INFO

Article history:
Received 26 March 2014
Accepted 12 June 2014
Available online 10 July 2014

Keywords:
CCHP
Deep-recovery
TEG
Exhaust gas
Simulation

ABSTRACT

Combined cooling, heating and power (CCHP) systems are thought to be highly efficient in energy utilization. But there are still potentials to further improve system performance. This work proposed a CCHP system based on internal combustion engine (ICE) for power generation, refrigeration and domestic hot water production. Thermoelectric generator (TEG) and condensing heat exchanger are applied to efficiently recover the exhaust gas waste heat of ICE. All the energy flows are designed based on energy cascading utilization principle. Basing on the test results of a 16 kW ICE, CCHP system characteristics are investigated by simulation from idling condition to full load condition. Especially, the part load performance of TEG and absorption chiller are simulated and discussed. The feasible operating zone of ICE and feed water flow rate are figured out to keep the domestic hot water temperature within a certain range. Results show that the primary energy efficiency of system can reach 0.944, thanks to the condensing heat recovery from exhaust gas. The primary energy saving ratio and cost saving ratio can reach 0.304 and 0.417, respectively. Considering some more equipment is incorporated, the total investment increment is about 11.1%.

1. Introduction

The application of combined heating and power has a history of more than 100 years, and it has grown into combined cooling, heating and power (CCHP) technology which is thought as a most advantageous branch of distributed generation [1–3]. Wu and Wang [3] and Caresana et al. [4] report that in CCHP system, especially in micro and small size system, internal combustion engine (ICE) is the most suitable prime mover, for its good adaptability, good reliability, and low initial investment. The efficiency of an ICE is usually inferior to that of a centralized power plant, even if considering the transmission loss of public grid. But the utilization of waste heat from ICE can make it be advantageous. So, it is quite significant to make the most of waste heat from ICE. At present, the reported primary energy efficiency of commonly used CCHP systems ranges from 0.5 to 0.86 [3,5–8]. Technically, there are potentials to further improve the performance of CCHP system.

Firstly, high efficient thermal activated devices should be used as much as possible. The exhaust gas temperature of ICE can be over 500 °C [5]. When there is cooling load, the exhaust gas can be used to power a double effect absorption chiller (DAC) directly. In many CCHP systems [5,9–12], exhaust gas is recovered by hot water, and then the hot water is used to power a single effect absorption chiller (*COP* of about 0.7 [13–15]), or an adsorption chiller (*COP* of 0.4–0.5 [13,16]). The *COP* of DAC powered by exhaust gas can range from 1.2 to 1.48 [15,17–19], which is obviously much higher efficient than other commonly used thermal activated devices. So DAC should be considered as much as possible.

Secondly, the exhaust gas can be used to power thermoelectric generator (TEG) for electricity generation instead of just heating hot water. The quality of electricity is much higher than that of hot water. Organic Rankine cycle is also a good choice to recover the waste heat of exhaust gas [20]. But the additional system is far more complex than TEG. Bass et al. have developed a TEG, which was installed outside the exhaust gas pipe of a truck and a capability of 1 kW power output was demonstrated [21,22]. Ikoma et al. [23] and Karri et al. [24] have also respectively studied TEG systems applied in exhaust gas waste heat recovery of engines. A TEG can be compactly integrated on the outside of exhaust gas pipe, and it could be feasible in a CCHP system.

Thirdly, exhaust gas deep-recovery can be applied to make the most of waste heat. The exhaust gas contains much gaseous water, especially for combustion of natural gas (NG). If the exhaust gas can be cooled below the dew point temperature (e.g. below 60 °C), not only much more sensible heat but also much condensing heat will be recovered. This concept is called as exhaust gas

* Corresponding author. Tel.: +86 21 3420 6776; fax: +86 21 3420 6814.
E-mail addresses: TJUgallon@sjtu.edu.cn (J.L. Wang), jywu@sjtu.edu.cn (J.Y. Wu), zhengchunyuan@sjtu.edu.cn (C.Y. Zheng).

http://dx.doi.org/10.1016/j.enconman.2014.06.036
0196-8904/

Nomenclature

a_0, a_1, a_2	polynomial fitting parameters
A	heat exchanger structure parameter
C	operation cost
c_p	specific heat at constant pressure (kJ/kg °C)
CCHP	combined cooling heating and power
COP	coefficient of performance
CHE	condensing heat exchanger
CSR	cost saving ratio
d	feature size of exhaust gas pipe (m)
DAC	double effect absorption chiller
ESR	energy saving ratio
F	heat exchange area (m^2)
f	function relationship
h	enthalpy (kJ/kg)
i	index number
j	index number
ICE	internal combustion engine
JHE	jacket water heat exchanger
k	heat transfer coefficient (kJ/m^2 °C)
L	latent heat of water (kJ/kg)
M	molar mass (kg/mol)
m	mass flow rate (kg/s)
N	number of TEG modules
n	molar quantity
NG	natural gas
Nu	Nusselt number
P	electric power (kW); pressure (Pa)
PEE	primary energy efficiency
PLR	part load ratio
Pr	Prandtl number
Pri	energy price
Q	thermal power (kW)
Re	Reynolds number
T	temperature (°C)
TAGS	a kind of material used in TEG
TEG	thermoelectric generator
zT	thermoelectric figure of merit of TEG

Subscript

b	boiler
c	cold side of TEG
con	conventional separated system
dew	dew point of exhaust gas
el	electricity
exh	exhaust gas
$fuel$	fuel consumption
fw	feed water
$grid$	public grid
jw	jacket water
h	hot side of TEG
$loss$	heat loss
i	inlet flow
m	exhaust gas state before entering CHE
o	outlet flow
$rated$	rated condition of ICE
sat	saturation state of water
vap	vapor state of water
w	water

Greek letter

ξ	energy price ratio
η	efficiency

deep-recovery [25], which can be realized by adding condensing heat exchanger (CHE). In fact, the condensing heat recovery of exhaust gas has been widely applied in condensing boiler in Europe, and the efficiency improvement is over 5% [26–28]. If deep-recovery is applied in CCHP system, the primary energy efficiency will be obviously enhanced.

Basing on above analyses, a framework of CCHP system is proposed for power generation, refrigeration and domestic hot water production. This paper proceeds as follow. Firstly, the principle of this CCHP system is described. Secondly, simulation models are developed and methodologies are introduced. Thirdly, system characteristics, performance are discussed. Finally, some main conclusions are summarized.

2. System description

Fig. 1 shows the schematic diagram of this CCHP system. Comparing with some commonly used CCHP systems [5–7,9–11,29–32], DAC is applied instead of single effect absorption chiller or adsorption chiller, TEG is applied instead of exhaust gas heat exchanger, and CHE is added to further recover the exhaust gas waste heat by deep-recovery process. Generally, heating load mainly includes house heating load and domestic hot water load. In this system, in order to realize exhaust gas deep-recovery, the feed water temperature should be low. The back water temperature from house heating cycle may be too high to realize exhaust gas deep-recovery. Therefore, a primary assumption is that only the domestic hot water load is satisfied by the CCHP system. Also, it can be understood that the existing hotels and residential buildings in the north of China have been equipped with central-heating system to specially meet the house heating load demand.

If valve 1 is turned on and valve 2 is turned off, the system will operate in combined heating and power mode (CHP mode). In CHP mode, the DAC is bypassed. So, there is no cooling output. The exhaust gas from ICE successively flows through TEG and CHE. In TEG, most of the sensible heat of exhaust gas is absorbed and electricity is generated. In CHE, the remained small part of sensible heat and some condensing heat of exhaust gas is recovered by deep-recovery process. Meanwhile, the feed water flows through CHE, TEG, and JHE in sequence (1–2–4–5–6) and turns into hot water. The hot water is entirely consumed as domestic hot water by user, so there is no circulating back water. Namely, the feed water should be from tap water which is cold. In CHE, the feed water absorbs the low temperature waste heat by deep-recovery process. And then it will be used as coolant water to cool the TEG. In TEG, only a small part of heat can be converted into electricity, while most of the absorbed heat is finally taken away by the coolant water in the cold side of TEG. So, the feed water can be further heated by the cold side of TEG. After flows through the TEG, the feed water flows into JHE and absorbs the whole waste heat in jacket water. In this way, the cold feed water is heated step by step and finally flows into the buffer tank.

If valve 1 is turned off and valve 2 is turned on, the system will operate in combined cooling, heating and power mode (CCHP mode). In CCHP mode, the TEG is bypassed. So there is no electric output from TEG. The exhaust gas from ICE flows into DAC for refrigeration, and then it flows into CHE for deep-recovery. In DAC, most of the sensible heat of exhaust gas is recovered. In CHE, the remained small part of low temperature sensible heat

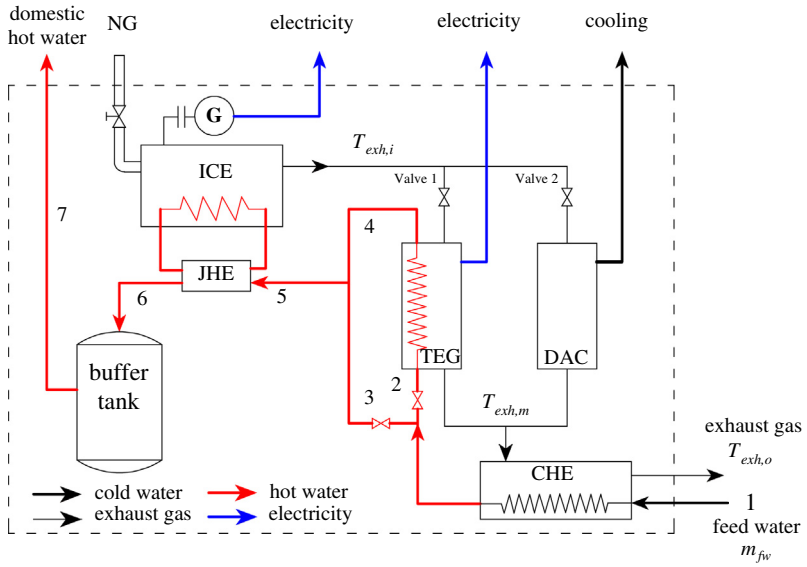

Fig. 1. Schematic diagram of CCHP system with exhaust gas deep-recovery and thermoelectric generator.

and some condensing heat of exhaust gas is recovered by deep-recovery process. Meanwhile, the feed water flows through CHE and JHE in sequence (1–3–5–6) and turns into hot water collected in buffer tank.

3. Modeling

3.1. ICE

The performance of ICE changes with the part load ratio of ICE (PLR_{ICE}). The PLR_{ICE} represents the operating state which is defined by the electric output and rated electric output of ICE, as:

$PLR_{ICE} = P_{el,ICE}/P_{el,ICE,rated}$. Some parameters, such as electric output, waste heat of jacket water, waste heat of exhaust gas, exhaust gas temperature, fuel consumption, and air consumption are all related with PLR_{ICE}. In this work, the relationships between these parameters and PLR_{ICE} are all tested by experiment. And these experimental parameters constitute the start point of the following simulation.

The fuel energy consumed by ICE is finally converted into electricity, waste heat, and heat loss. So the energy balance in ICE is:

$$Q_{fuel,ICE} = P_{el} + Q_{jw} + Q_{exh} + Q_{loss} \tag{1}$$

$$T_{w,6} = T_{w,5} + \frac{Q_{jw}}{c_{p,w} \cdot m_{fw}} \tag{2}$$

The hot water outlet temperature after JHE in state 6 is calculated as:where, the hot water temperature in state 5 can be got in the following simulation.

3.2. DAC

The DAC applied in this work is a lithium bromide water ($LiBr-H_2O$) type with the high pressure generator and low pressure generator in parallel. The condensing heat of refrigerant vapor from high pressure generator is used to power the low pressure generator firstly, and then part of its sensible heat is further recovered by low pressure heat exchanger. This type of structure can be referred to [33]. In simulation, the high pressure generator of DAC is powered by exhaust gas directly, and the DAC is cooled by a cooling tower. As powered by the waste heat of exhaust gas from ICE, the performance of DAC depends on PLR_{ICE}. So, the simulation will be conducted under various PLR_{ICE}. The rated condition of DAC is designed based on the exhaust gas condition with PLR_{ICE} of 1.

In off-design operation, the heat transfer performance of high pressure generator changes with the mass flow rate and temperature of exhaust gas. This kind of relationship can be simply related by [34]:

$$kF = Am_{exh}^{0.6}T^r \tag{3}$$

where k is the heat transfer coefficient, A is a parameter related to the heat exchanger structure, m_{exh} is the mass flow rate of exhaust gas, r is a factor considering the influence of thermo-physical properties of exhaust gas. r can be estimated by:

$$r = 0.67s - 0.27l \tag{4}$$

where s and l are the powers of heat conductivity coefficient and kinematic viscosity with temperature, respectively.

The total mass balance, solute mass balance and energy balance equations for each component of DAC can be respectively represented as:

$$\sum m_i - \sum m_o = 0 \tag{5}$$

$$\sum m_i w_i - \sum m_o w_i = 0 \tag{6}$$

$$Q + \sum m_i h_i - \sum m_o h_o = 0 \tag{7}$$

where the subscript i and o mean inlet flow and outlet flow, respectively.

The heat transmission in each component of DAC can be calculated by:

$$Q = kF\Delta T \tag{8}$$

where ΔT is the logarithmic mean temperature difference. In high pressure generator, kF can be calculated by Eq. (3). In any other component, the temperature fluctuation is small and kF can be assumed as constant which can be calculated by simulation in rated condition.

All the thermodynamic properties of $LiBr–H_2O$ solution used in simulation come from results of [35]. Some other commonly applied equations and assumptions in simulation can be referred to [33] and [36]. By simulation, the exhaust gas outlet temperature

$T_{exh,m}$, refrigeration *COP*, and some other results under various PLR_{ICE} can be calculated.

The heat consumption by DAC is calculated by:

$$Q_{DAC} = c_{p,exh} m_{exh} (T_{exh,i} - T_{exh,m}) \tag{9}$$

The cooling output of DAC is calculated by:

$$Q_c = COP_{DAC} \cdot Q_{DAC} \tag{10}$$

3.3. TEG

TEG is a device that converts thermal power into electric power based on the principle of Seebeck effect [37]. If there is a temperature difference between the hot side and cold side of TEG, there will be electric current through the TEG. TEG usually consists of many TEG modules. The transport characteristics of a TEG module can be represented by the thermoelectric figure of merit (zT). For a given material, the efficiency of a TEG module depends of the temperature condition, which can be calculated as [38]:

$$\eta = \frac{\Delta T}{T_h + 273.15} \cdot \frac{\sqrt{1 + \overline{zT}} - 1}{\sqrt{1 + \overline{zT}} + \frac{T_c + 273.15}{T_h + 273.15}} \tag{11}$$

where $\overline{zT}$ is the thermoelectric figure of merit calculated at mean temperature between hot side and cold side.

Similar to a heat engine, the theoretical maximum electric efficiency of a TEG module is limited by the Carnot efficiency, namely $\Delta T/(T_h + 273.15)$. A larger zT will help to increase the efficiency under a given temperature condition. In this work, TAGS, which has been successfully used in long-life thermoelectric generators, is used as the TEG module material. Snyder et al. presented a function curve for zT of TAGS with temperature [38]. Herein, this functional relationship is approximately described by a polynomial fitting equation as:

$$zT(T) = a_2 \cdot T^2 + a_1 \cdot T + a_0 \tag{12}$$

where a_2, a_1 and a_0 are −6.879e−6, 6.443e−3, and −0.3498, respectively.

Technically, the TEG modules usually distribute around the exhaust gas pipe as some products show [22]. The hot side of a TEG module contacts with the exhaust gas. The Nusselt number of heat transfer can be estimated by the Dittus–Boelter formula as [39]:

$$Nu = 0.023 Re^{0.8} Pr^{0.3} \tag{13}$$

As the hot side temperature changes along the exhaust gas flow, the performance of a TEG module depends on the local condition. The heat absorbed by the hot side of a TEG module is:

$$Q_{TEG,i} = \frac{Nu\lambda}{d} F (T_{exh,i} - T_{h,i}) \tag{14}$$

where i represents ith TEG module, $i = 1,\ldots, N$. The total electric output of TEG should be calculated as:

$$P_{TEG} = \sum_{i=1}^{N} \eta_{TEG,i} Q_{TEG,i} \tag{15}$$

In turn, the efficiency of TEG device should be calculated as:

$$\eta_{TEG} = \frac{P_{TEG}}{c_{p,exh} m_{exh} (T_{exh,i} - T_{exh,m})} \tag{16}$$

Then, the heat absorbed by the coolant water in the cold side of TEG can be calculated as:

$$Q_{TEG,c} = \eta_c (Q_{TEG,h} - P_{TEG}) \tag{17}$$

where heat recovery efficiency η_c in cold side of TEG is assumed as 0.9 considering heat loss in TEG.

The feed water absorbs the heat from the cold side of TEG and then the water temperature increases from state 2 to state 4:

$$T_{w,4} = T_{w,2} + \frac{Q_{TEG,c}}{c_{p,w} \cdot m_{fw}} \tag{18}$$

3.4. Exhaust gas deep-recovery

For a given combustion condition, including fuel composition and air consumption rate, the exhaust gas composition can be calculated. Once the exhaust gas composition is known, the condensation characteristics can be analyzed. Herein, it is assumed that the fuel is completely burned. And the exhaust gas is assumed as ideal gas, which consists of O_2, CO_2, N_2 and H_2O.

The dew point temperature T_{dew} of exhaust gas depends on the partial pressure of gaseous water P_{vap}.

For ideal gas, P_{vap} can be calculated by the mole fraction as:

$$P_{vap} = P_{exh} \cdot n_{vap}/n_{exh} \tag{19}$$

where n_{vap} is the molar quantity of gaseous water, n_{exh} is the molar quantity of exhaust gas, and both of them can be calculated according to the chemical equation of combustion. The higher the gaseous water content is, the higher the dew point temperature will be. The relationship between dew point temperature and partial pressure of gaseous water can be associated by:

$$T_{dew} = f_{vap}(P_{vap}) \tag{20}$$

where f_{vap} represents the thermodynamic function for gaseous water, which can be calculated by REFPROP [40].

The gaseous water content before CHE can be calculated by:

$$m_{vap,m} = n_{vap} \cdot M_{vap} \tag{21}$$

where M_{vap} is the molar mass of water.

And the gaseous water content after CHE can be calculated by:

$$m_{vap,o} = \frac{p_{sat,o}}{p_{exh,o}} \cdot n_{exh,o} \cdot M_{vap} \tag{22}$$

where $P_{sat,o}$ is the saturation pressure of gaseous water corresponding to the dew point of exhaust gas after CHE. Then the mass of condensed water m_{dew} can be got by:

$$m_{dew} = m_{vap,m} - m_{vap,o} \tag{23}$$

The recoverable waste heat in the process of deep-recovery is calculated by:

$$Q_{CHE} = \sum_{j=1}^{4} m_j \cdot (h_{j,m} - h_{j,o}) + m_{dew} \cdot L \tag{24}$$

where $j = 1, 2, 3, 4$ corresponds to O_2, CO_2, N_2, and H_2O in gaseous state, respectively. L is the latent heat of phase change of water.

The feed water is firstly heated by CHE and then the water temperature increases to state 2 (or 3):

$$T_{w,2} = T_{w,1} + Q_{CHE}/(c_{p,w} \cdot m_{fw}) \tag{25}$$

3.5. Performance evaluation

Primary energy efficiency (*PEE*) is used to describe the total efficiency of CCHP system based on the first law of thermodynamics. It represents the ratio of the whole energy output to primary energy consumption (lower heating value) [5].

$$PEE = \frac{P_{el} + Q_c + Q_h}{Q_{fuel,CCHP}} \tag{26}$$

Primary energy saving ratio (*ESR*) and cost saving ratio (*CSR*) are widely used to evaluate the performance of CCHP system compared with conventional separated system [41]. The *ESR* is defined as:

$$ESR = \frac{Q_{fuel,con} - Q_{fuel,CCHP}}{Q_{fuel,con}} \quad (27)$$

Typically, conventional separated system is assumed as: the electric load is satisfied by the public grid, the cooling load is satisfied by an electric chiller, and the heating load is satisfied by a gas boiler. So, the fuel consumption of conventional separated system is calculated by:

$$Q_{fuel,con} = \frac{P_{el} + Q_c/COP_{el,chiller}}{\eta_{grid}} + \frac{Q_h}{\eta_b} \quad (28)$$

Similarly, the *CSR* is defined as:

$$CSR = \frac{C_{con} - C_{CCHP}}{C_{con}} \quad (29)$$

The operation cost is defined according to the cost by energy consumption:

$$C = P_{el,grid}Pri_{el} + (Q_{fuel,b} + Q_{fuel,ICE})Pri_{fuel} \quad (30)$$

where $Q_{fuel,b}$ and $P_{el,grid}$ are both 0 for CCHP system, $Q_{fuel,ICE}$ is 0 for conventional separated system.

So, Eq. (29) can be calculated as:

$$CSR = \frac{(P_{el,grid} + \xi \cdot Q_{fuel,b})_{con} - (\xi \cdot Q_{fuel,ICE})_{CCHP}}{(P_{el,grid} + \xi \cdot Q_{fuel,b})_{con}} \quad (31)$$

where ξ is the energy price ratio defined as $\xi = Pri_{fuel}/Pri_{el}$ [40].

4. Results and discussion

4.1. Exhaust gas deep-recovery

A 16 kW ICE is tested and some related experimental results are listed in Table 1. The ICE is tested from idling condition to full load condition, with PLR_{ICE} changes from 0 to 1. The exhaust gas temperature increases with PLR_{ICE}, and it reaches 670.4 °C at full load condition.

Table 2 shows the composition of NG. The content of CH_4 is 97.92%. So, there will be much gaseous water contained in the exhaust gas of NG. In deep-recovery, most of the gaseous water can be condensed and the condensing heat can be recovered by cold feed water. Basing on the NG consumption rate, air flow rate, and fuel composition, the dew point and condensing heat of exhaust gas can be calculated. As shown in Fig. 2, the condensing heat changes from 1.37 to 4.4 kW when the PLR_{ICE} changes from 0.1 to 1. The corresponding dew point temperature of exhaust gas changes from 54.7 to 57.1 °C, which is a little lower than the result calculated by Che et al. [26]. As the air factor in their studied condition is lower than this work, they concluded that the dew point temperature is generally 56–60 °C.

The recoverable waste heat in deep-recovery includes sensible heat and condensing heat. Fig. 3 shows the recoverable waste heat of ICE and total recoverable waste heat increasing rate by deep-recovery. As the PLR_{ICE} increases from 0.1 to 1, the waste heat of jacket water varies from 11.2 kW to 22.3 kW, and the waste heat of exhaust gas (>100 °C) varies from 4.97 to 14.2 kW. If the exhaust gas is further cooled to 40 °C by deep-recovery (It has been realized in a preliminary test by 20 °C feed water), much more waste heat can be recovered as the white columns show. It makes the recoverable exhaust gas waste heat and total recoverable waste heat increase by 41–46% and 13–16%, respectively. So, exhaust gas deep-recovery can greatly improve the energy utilization efficiency.

Table 1
Experimental results of a 16 kW ICE[a].

PLR_{ICE}	NG consumption rate ($N m^3/h$)	Air flow rate ($N m^3/h$)	Exhaust gas temperature (°C)
0	2.01	26.44	439.46
0.1	2.32	31.60	473.9
0.2	2.56	34.77	480.95
0.3	2.88	39.29	512.36
0.4	3.25	43.28	523.39
0.5	3.75	48.12	548.93
0.6	4.25	52.11	567.5
0.7	4.78	57.78	594.87
0.8	5.4	64.29	603.3
0.9	6.07	73.95	627.95
1	6.76	84.67	670.4

[a] The type of ICE is Cummins GGDB16.

4.2. Performance in CCHP mode

Fig. 4 shows the part load ratio performance of system in CCHP mode. As the TEG does not operate, all the electric output comes from ICE and the maximum electric output is 16 kW. The cooling output increases from 6.14 kW to 17.56 kW while the heating output increases from 12.9 kW to 30.31 kW. It means that, even in CCHP mode, the heating output is obviously much more than the cooling output. So, this kind of CCHP system is suitable for users with large domestic hot water demand. Analysis shows that, 13.3–19.5% fuel energy (lower heating value) is lost to the environment in this system, but deep-recovery of exhaust gas contributes some other condensing heat which does not count in the lower heating value. In addition, the *COP* of DAC is great than 1, which also magnifies the thermal output. So, the average *PEE* reaches 0.944 as shown in Fig. 4. The theoretical *PEE* can be expected to be over 1 if condensing heat is recovered as much as possible.

Fig. 5 shows the influence of PLR_{ICE} on performance of DAC. Both the exhaust gas outlet temperature after DAC and thermal *COP* are investigated. In the rated condition with PLR_{ICE} of 1, the exhaust gas outlet temperature is designed at 170 °C. If PLR_{ICE} decreases to 0, namely in idling condition, the exhaust gas outlet temperature will decreases to 107 °C. Simultaneously, the *COP* of DAC presents a trend of parabolic curve. The *COP* of DAC reaches maximum when the PLR_{ICE} is less than 1, which means that the best heat and mass transfer performance of DAC is not in full load condition. Zheng et al. [34] and Wu et al. [42] have also respectively pointed out that the best performance of DAC and ICE may not in full load condition.

The hot water to the buffer tank represents the whole heating output. Obviously, the hot water outlet temperature is important for user. As shown in Fig. 6, it is the contour map of hot water outlet temperature in CCHP mode, considering the influence of PLR_{ICE} and feed water flow rate. The orange zone, which is named as feasible operating zone, represents hot water outlet temperature ranging between 45 °C and 85 °C. These two temperature values are assumed artificially. A lower temperature may be unacceptable by user. A higher temperature may influence the cooling of jacket water cycle and damage the ICE. For a given PLR_{ICE}, which means the waste heat is given, the hot water outlet temperature increases as the feed water flow rate decreases. For a given feed water flow rate, the hot water outlet temperature increases with PLR_{ICE}. It can be found that the hot water outlet temperature will be always within the assumed temperature range if the feed water flow rate is set between 0.4 m^3/h and 0.44 m^3/h.

4.3. Performance in CHP mode

Fig. 7 shows the part load ratio performance of system in CHP mode. As the DAC does not operate, there is no cooling output. The electric output comes from the ICE and TEG simultaneously. Both the electric output and heating output increase with the PLR_{ICE}. The electric output of system reaches 17.18 kW when PLR_{ICE} is 1, in which 16 kW comes from ICE and the extra 1.18 kW comes from TEG. The heating output comes from the released heat of the cold side of TEG, the waste heat of exhaust gas in deep-recovery,

Table 2
Composition of NG.

Contents	CO_2	N_2	CH_4	C_2H_6	C_3H_8	C_4H_{10}	C_5H_{12}	C_6
Percentage (%)	0.657	0.72	97.92	0.561	0.058	0.037	0.013	0.034

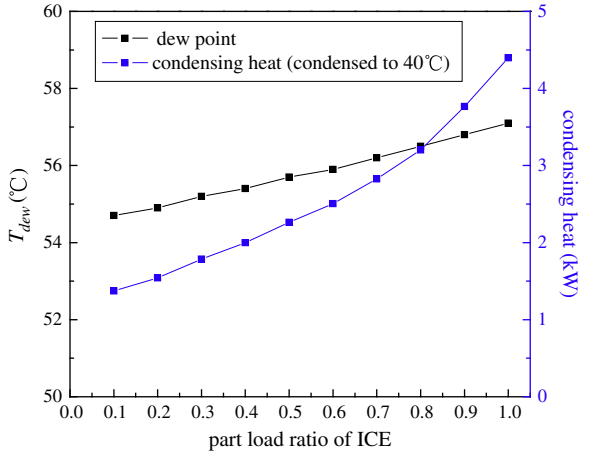

Fig. 2. Dew point and condensing heat of exhaust gas.

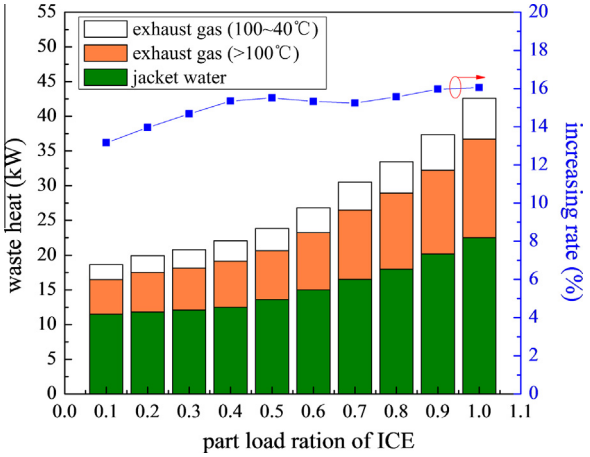

Fig. 3. Recoverable waste heat of ICE and total recoverable waste heat increasing rate by deep-recovery.

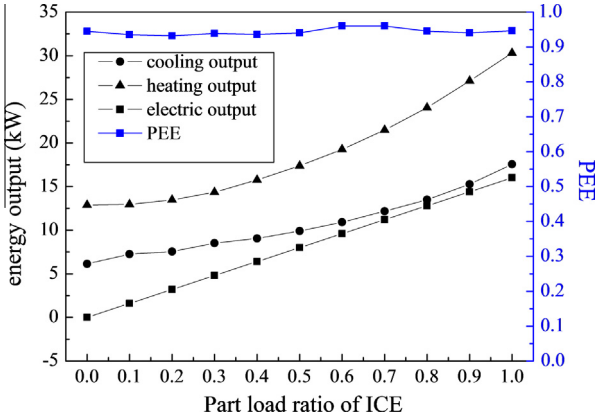

Fig. 4. Part load ratio performance of system in CCHP mode.

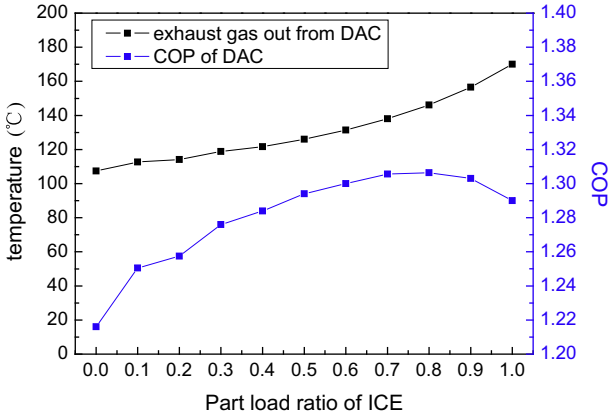

Fig. 5. Influence of PLR_{ICE} on performance of DAC.

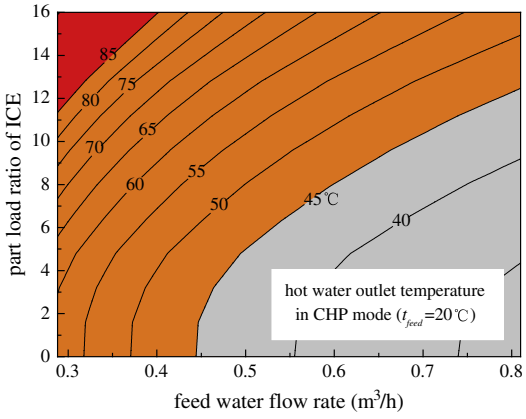

Fig. 6. Contour map of hot water outlet temperature in CCHP mode.

and the waste heat of jacket water. It can be found that the average *PEE* reaches 0.908. This value agrees with the result reported by Fu et al. [43]. In their experiment, by recovering the jacket water waste heat, sensible heat of exhaust gas and condensing heat of exhaust gas for heating, the *PEE* reaches about 90–94%.

Fig. 8 shows the influences of PLR_{ICE} on electric output of TEG and electric efficiency of CCHP system. It can be found that the electric output of TEG increases with PLR_{ICE}. The minimum electric output of TEG is 0.23 kW, which occurs when the ICE operates in idling condition with PLR_{ICE} of 0.The maximum electric output of TEG is 1.18 kW, which occurs when the ICE operates in full load condition with PLR_{ICE} of 1. As a demonstration, Bass et al. have realized 1 kW power output by installing a TEG device outside the exhaust gas pipe of a truck [21]. As TEG is applied, the electric efficiency of CCHP system is improved. When the PLR_{ICE} is 1, the electric efficiency is improved from 0.237 to 0.254 with increasing rate of 7.4%.

Fig. 9 shows the influence of PLR_{ICE} on performance of TEG. Both the exhaust gas outlet temperature after TEG and electric efficiency of TEG are investigated. In the rated condition with PLR_{ICE} of 1, the exhaust gas outlet temperature is designed to be 170 °C. Both the exhaust gas outlet temperature and electric efficiency increases with PLR_{ICE}. If PLR_{ICE} decreases to 0, namely the ICE operates in

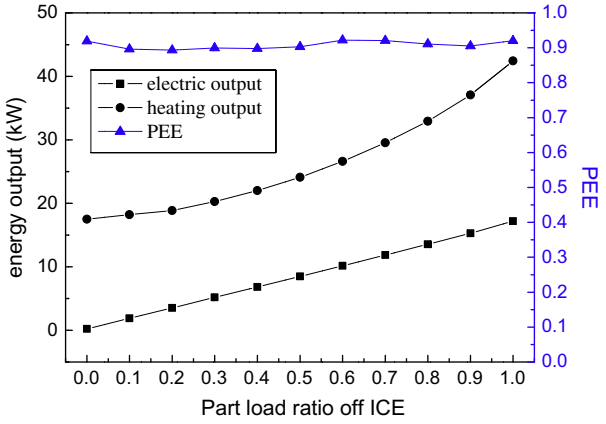

Fig. 7. Part load ratio performance of system in CHP mode.

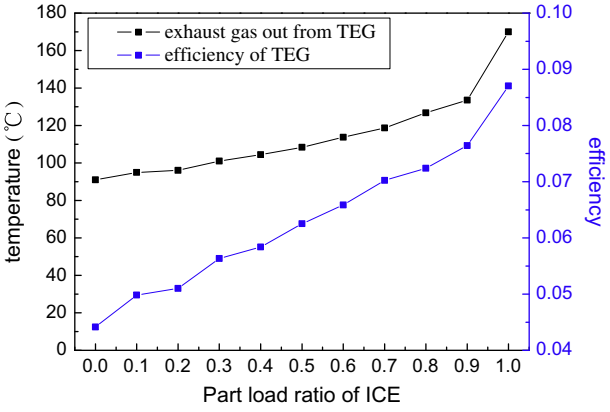

Fig. 9. Influence of PLR_{ICE} on performance of TEG.

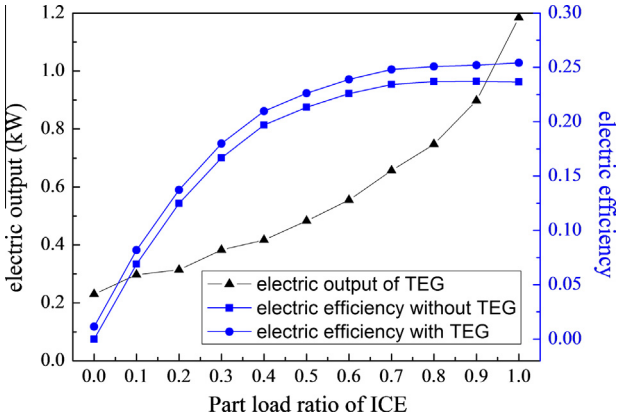

Fig. 8. Influences of PLR_{ICE} on electric output of TEG and electric efficiency of CCHP system.

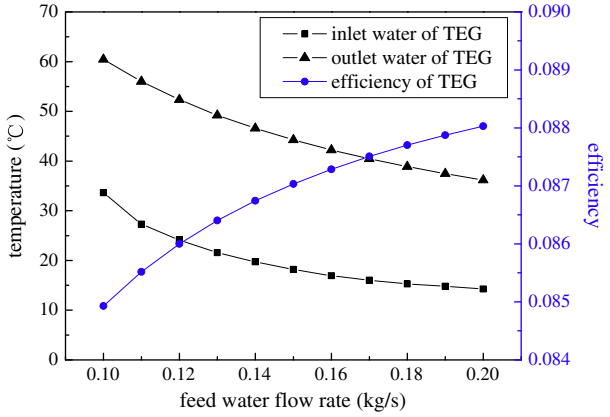

Fig. 10. Influence of feed water flow rate on the performance of TEG (PLR_{ICE} = 1).

idling condition, the outlet temperature will decrease to 91 °C. The electric efficiency of TEG can reach 0.087 and 0.044 with PLR_{ICE} of 1 and 0, respectively. In comparison, the efficiencies are reported at 0.09 and 0.065 based on module material of ECO21 for the same temperature differences, respectively [44]. So, the performance of TEG is greatly influenced by PLR_{ICE}. A higher PLR_{ICE} means higher exhaust gas temperature and flow rate from ICE, which can improve the performance of TEG.

Fig. 10 shows the influence of feed water flow rate on the performance of TEG with PLR_{ICE} of 1. A larger feed water flow rate can help to cool the cold side of TEG and improve the performance of TEG. So, the electric efficiency of TEG increases with the flow rate. Simultaneously, the water outlet temperature of TEG decreases as the feed water flow rate increases. So, a larger flow rate will result in a lower hot water outlet temperature. There should be a feasible range of feed water flow rate.

As Figs. 11 and 12 show, they are the contour maps of hot water outlet temperature in the transitional season condition and winter season condition, respectively. According to the typical tap water temperature, the feed water temperatures in the transitional season and winter season are assumed at 12 °C and 5 °C, respectively. As the orange feasible operating zone shows, too large or too small feed water flow rate will shrink the feasible operating range of PLR_{ICE}. For the transitional season condition, a flow rate of 0.45–0.5 m^3/h will be the most adaptive. For the winter season condition, a flow rate of 0.38–0.47 m^3/h can be considered. If the hot water should be temporarily stored in the buffer tank, the flow rate can be controlled as low as possible to increase the stored hot water temperature.

4.4. System evaluation

Fig. 13 shows the influence of PLR_{ICE} on *ESR*. As the black curves show, system operations without TEG and CHE are used for comparisons. The *ESRs* of CCHP mode and CHP mode are similar to each other. But, there is obvious difference for *ESR* between systems with and without TEG and CHE. Especially in CHP mode with PLR_{ICE} of 1, the *ESR* is improved from 0.216 to 0.304 by applying TEG and CHE. When the PLR_{ICE} is over 0.5, the *ESR* of CCHP system is about 0.28 while it is only about 0.21 without TEG and CHE. So, as TEG and CHE are applied, much more energy can be saved. Once the PLR_{ICE} is below 0.5, the system performances dramatically get worse. This similar trend also occurs to CCHP system without TEG and CHE. So, CCHP systems are recommended to be operated with high PLR_{ICE}.

Fig. 14 shows the influence of PLR_{ICE} on *CSR*. In CCHP mode, the *CSR* of system is about 0.04–0.09 higher than system without TEG and CHE. In CHP mode, it is about 0.05–0.12. For CHP mode with PLR_{ICE} of 1, the *CSR* of system reaches 0.417 while it is 0.349 without TEG and CHE. So, by applying TEG and CHE, the system operation can become much more economical.

Further considering a floating energy price, Fig. 15 shows the sensitivity analysis of energy price ratio on *CSR*. The theoretical maximum *CSR* is 1 with energy price ratio of 0, namely the fuel price is 0 or the electric price is infinitely great. A higher fuel price means a worse economical performance of CCHP system operation. So, the *CSR* decreases as the energy price ratio increases. The continuous curves represent the performances of CCHP system, and the dash curves represent the performances of CCHP system without TEG and CHE. The red dash lines indicate the present local case

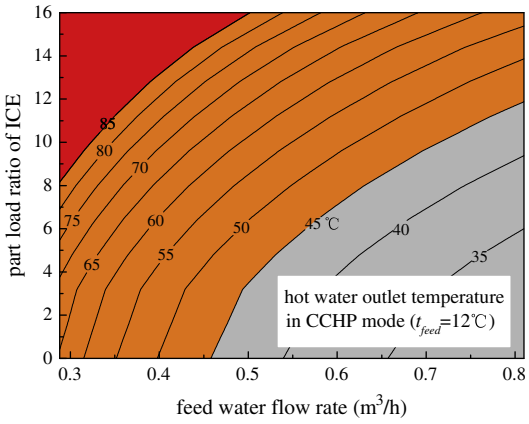

Fig. 11. Contour map of hot water outlet temperature in the transitional season condition.

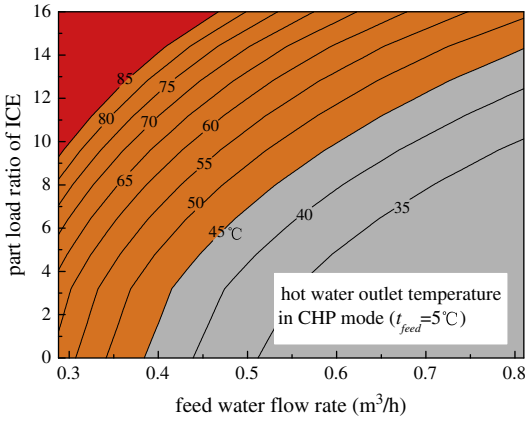

Fig. 12. Contour map of hot water outlet temperature in winter season condition.

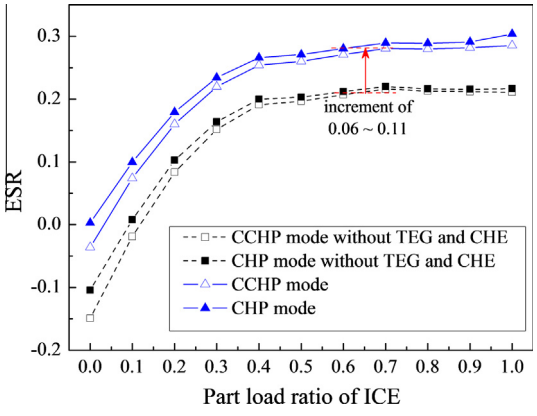

Fig. 13. Influence of PLR_{ICE} on *ESR*.

with energy price ratio of 0.25. The red points marked on the *X* axis show the energy price ratios with *CSR* of 0. They are named as critical *CSRs*. If TEG and CHE are not applied, the critical *CSRs* in CCHP mode and CHP mode are 0.49 and 0.58, respectively. If TEG and CHE are both applied, the critical *CSRs* in CCHP mode and CHP mode get much higher and they are 0.62 and 0.84, respectively. Obviously, the economical adaptability is greatly improved.

As TEG and CHE are incorporated, the initial investment should be higher. Table 3 shows the investments of related devices and system integration fees. Basing on Table 3, Fig. 16 shows the

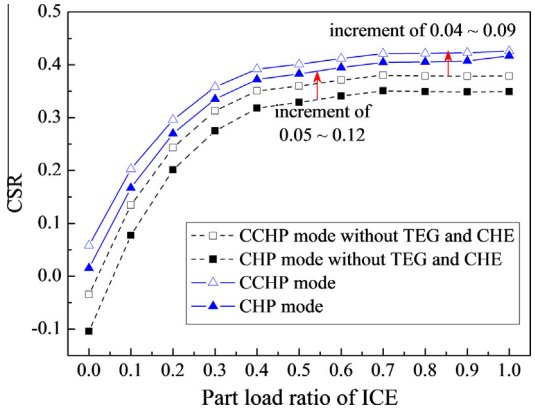

Fig. 14. Influence of PLR_{ICE} on *CSR*.

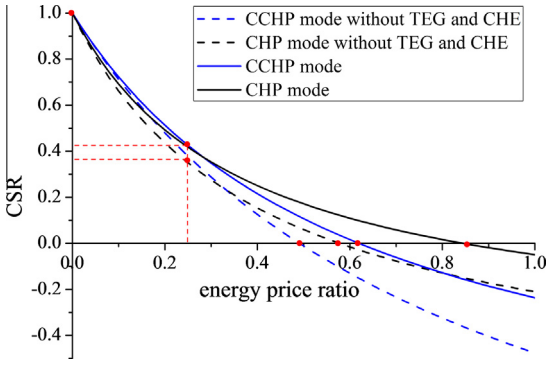

Fig. 15. Sensitivity analysis of energy price ratio on *CSR* (PLR_{ICE} = 1).

Table 3
Prices and investments of every involved device.

Items	Price ($/kW)	Capacity (kW)	Investment ($)
DAC	900	18	16,200
ICE-G	800	16	12,800
TEG	2000	1.2	2400
CHE	70 [45]	9	630
JHE	10	23	230
System integration without TEG and CHE	–	–	7000[a]
System integration with TEG and CHE	–	–	8000[b]

[a] Considering the cost of control system, pipes, valves, and so on.
[b] Including the increased investment of exhaust gas heat exchanger needed by TEG.

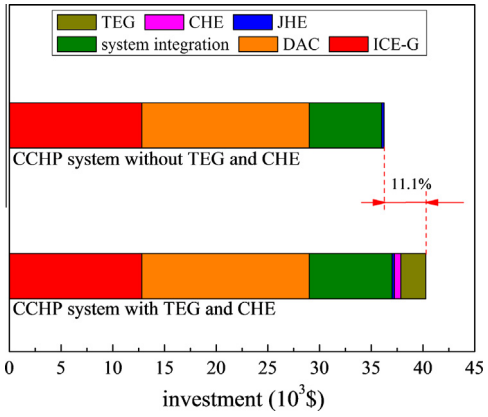

Fig. 16. Investments comparison between systems with and without TEG and CHE.

investments comparison between systems with and without TEG and CHE. It can be found that, the total investment is mainly caused by the ICE and DAC. Although the present TEG price for per kW is very high, the required capacity is small. So, the total investment increment of system is about 11.1%.

5. Conclusions

A CCHP system is proposed for power generation, refrigeration, and domestic hot water production. The operating characteristics under various working conditions are simulated and discussed. This kind of CCHP system shows an obviously better performance with some increment of total investment. Some main conclusions are summarized as follows.

Firstly, as deep-recovery of exhaust gas is applied, the total recoverable waste heat of CCHP system is improved by 13–16%. The *PEE* of CCHP system reaches 0.944 and 0.908 in CCHP mode and CHP mode, respectively.

Secondly, as TEG is applied to generate electricity by waste heat, the CCHP system can realize a higher electric efficiency. When PLR_{ICE} is 1, the electric efficiency is improved from 0.237 to 0.254 with increasing rate of 7.4%.

Thirdly, there is a feasible operating zone in order to control the hot water outlet temperature between 45 °C and 85°C. According to the contour maps of hot water outlet temperature, the feasible controlling strategy of ICE and feed water flow rate can be found.

Fourthly, the system performance improvement is obvious by applying TEG and CHE. For CHP mode with PLR_{ICE} of 1, the *ESR* is improved from 0.216 to 0.304, and the *CSR* is improved from 0.349 to 0.417. In addition, the economical adaptability is also greatly improved, and the total investment increment of CCHP system is 11.1%.

Acknowledgement

This work is supported by National Natural Science Foundation of China, (No. 51076099).

References

[1] Xu JZ, Sui J, Li BY, et al. Research, development and the prospect of combined cooling, heating, and power systems. Energy 2010;35:4361–7.
[2] Dong LL, Liu H, Riffat S. Development of small-scale and micro-scale biomass-fuelled CHP systems – a literature review. Appl Therm Eng 2009;29:2119–26.
[3] Wu DW, Wang RZ. Combined cooling heating and power: a review. Prog Energy Combust Sci 2006;32:459–95.
[4] Caresana F, Brandoni C, Feliciotti P, et al. Energy and economic analysis of an ICE-based variable speed-operated micro-cogenerator. Appl Energy 2011;88:659–71.
[5] Kong XQ, Wang RZ, Wu JY. Experimental investigation of a micro-combined cooling heating and power system driven by a gas engine. Int J Refrig 2005;28:977–87.
[6] Khatri KK, Sharma D, Soni SL, et al. Experimental investigation of CI engine operated micro-trigeneration system. Appl Therm Eng 2010;30:1505–9.
[7] Onovwiona HI, Ismet Ugursal V, Fung Alan S. Modeling of internal combustion engine based cogeneration systems for residential applications. Appl Therm Eng 2007;27:848–61.
[8] Fumo N, Mago PJ, Jacobs K. Design considerations for combined cooling, heating, and power systems at altitude. Energy Convers Manage 2011;52:1459–69.
[9] Jing YY, Bai H, Wang JJ. Multi-objective optimization design and operation strategy analysis of BCHP system based on life cycle assessment. Energy 2012;37:405–16.
[10] Wang JJ, Zhai ZQJ, et al. Environmental impact analysis of BCHP system in different climate zones in China. Energy 2010;35:4208–16.
[11] Ebrahimi M, Keshavarz A. Sizing the prime mover of a residential micro-combined cooling heating and power (CCHP) system by multi-criteria sizing method for different climates. Energy 2013;54:291–301.
[12] Giffin PK. Performance and cost results from a DOE Micro-CHP demonstration facility at Mississippi State University. Energy Convers Manage 2013;65:364–71.
[13] Deng J, Wang RZ, Han GY. A review of thermally activated cooling technologies for combined cooling heating and power systems. Prog Energy Combust Sci 2011;37:172–203.
[14] Jiangsu Huineng New Energy Technology Co., Ltd. Small Type Hot Water Absorption Chiller Parameters, 2014.<http://www.tynkt.com/en/param_rxz.asp>.
[15] Gomri R. Investigation of the potential of application of single effect and multiple effect absorption cooling systems. Energy Convers Manage 2010;51:1629–36.
[16] Wu JY, Li S. Study on cyclic characteristics of silica gel-water adsorption cooling system driven by variable heat source. Energy 2009;34:1955–62.
[17] Marcos JD, Izquierdo M, Palacios E. New method for COP optimization in water- and air-cooled single and double effect LiBr-water absorption machines. Int J Refrig 2011;34:1348–59.
[18] Broad Group. BROAD X Non-electric Chiller, 2014 <http://www.broad.com/uploads/pdf/xxfiktxxsjsc.pdf>.
[19] Gomri R, Hakimi R. Second law analysis of double effect vapor absorption cooler system. Energy Convers Manage 2008;49:3343–8.
[20] Fang F, Wei L, Liu JZ. Complementary configuration and operation of a CCHP-ORC system. Energy 2012;46:211–20.
[21] Bass JC, Elsner NB, Leavitt FA. Performance of l kW thermoelectric generator for diesel engines. In: Proc. 23rd International Conference on Thermoelectrics 1994, p. 295–8.
[22] Hi-Z technology Inc. hi-z_applications, 2014 <http://www.hi-z.com/uploads/2/3/0/9/23090410/hi-z_applications.pdf>.
[23] Ikoma K, Munekiyo M, Furuya K et al. Thermoelectric module and generator for gasoline engine vehicles. In: 17th International Conference on Thermoelectrics. Nagoya, Japan; 1998, p. 464–67.
[24] Karri MA, Thacher EF, Helenbrook BT. Exhaust energy conversion by thermoelectric generator: two case studies. Energy Convers Manage 2011;52:1596–611.
[25] Wang JL, Wu JY. Deep-recovery schemes of waste heat in flue gas and cost analysis of optimum model. CIESC J. 2012;63:1529–35 [in Chinese].
[26] Che DF, Liu YH, Gao CY. Evaluation of retrofitting a conventional natural gas fired boiler into a condensing boiler. Energy Convers Manage 2004;45:3251–66.
[27] Fu L, Tian GS, Sui J, et al. Combining absorption heat pump with gas boiler for exhaust condensing heat recovery in district heating system. Acta Energiae Solaris Sinica 2003;24:620–4.
[28] Boeschen PL. A case study of condensing boiler energy savings. AHRAE Trans 2000;Part 1:96–105.
[29] Lee H, Bush J, Hwang Y. Modeling of micro-CHP (combined heat and power) unit and evaluation of system performance in building application in United States. Energy 2013;58:364–75.
[30] Deng J, Wang RZ, Wu JY, et al. Exergy cost analysis of a micro-trigeneration system based on the structural theory of thermoeconomics. Energy 2008;33:1417–26.
[31] Rocha MS, Andreos R, Simões-Moreira JR. Performance tests of two small trigeneration pilot plants. Appl Therm Eng 2012;41:84–91.
[32] Li S, Wu JY. Theoretical research of a silica gel-water adsorption chiller in a micro combined cooling, heating and power (CCHP) system. Appl Energy 2009;86:958–67.
[33] Wang L, Chen GM, Wang Q, Zhong M. Thermodynamic performance analysis of gas-fired air-cooled adiabatic absorption refrigeration systems. Appl Therm Eng 2007;27(8):1642–52.
[34] Zheng JJ, Guo PJ, Sui J, et al. Off-design performance of an exhaust-fired absorption refrigerator. J Eng Thermophys 2012;33(8):1275–8 [in Chinese].
[35] Pátek J, Klomfar J. A computationally effective formulation of the thermodynamic properties of LiBr–H_2O solutions from 273 to 500 K over full composition range. Int J Refrig 2006;29:566–78.
[36] Dai YQ. Lithium Bromide Absorption Chiller: Technology and Applications. Beijing: Mechanical Industry Publishers; 1996 [in Chinese].
[37] Riffat SB, Ma XL. Thermoelectrics: a review of present and potential applications. Appl Therm Eng 2003;23:913–35.
[38] Jeffrey Snyder G, Toberer Eric S. Complex thermoelectric materials. Nat Mater 2008;7(2):105–14.
[39] Lotfi R, Saboohi Y, Rashidi AM. Numerical study of forced convective heat transfer of Nanofluids: comparison of different approaches. Int Commun Heat Mass Transfer 2010;37:74–8.
[40] Lemmon EW, McLinden MO, Huber ML. NIST reference fluid thermodynamic and transport properties-REFPROP. NIST standard reference database 23-Version 7.0.
[41] Wu JY, Wang JL, Li S. Multi-objective optimal operation strategy study of micro-CCHP system. Energy 2012;48:472–83.
[42] Wu JY, Wang JL, Li S, et al. Experimental and simulative investigation of a micro-CCHP (micro combined cooling, heating and power) system with thermal management controller. Energy 2014;68:444–53.
[43] Fu L, Zhao XL, Zhang SG, et al. Performance study of an innovative natural gas CHP system. Energy Convers Manage 2011;52:321–8.
[44] Kajikawa T, Ozaki M, Yamaguchi K et al. Progress of Development for Advanced Thermoelectric Conversion Systems. In: 24th International Conference on Thermoelectrics. 2005, p. 162–9.
[45] Weiss M, Dittmar L, Junginger M, et al. Market diffusion, technological learning, and cost-benefit dynamics of condensing gas boilers in the Netherlands. Energy Policy 2009;37:2962–76.